Two-Phase Flow Simulations in a Natural Rock Fracture using the VOF Method

D. Crandall[1], G. Ahmadi[2], D.H. Smith[3], and G. Bromhal[4]

[1]URS Washington Division, National Energy Technology Laboratory
Morgantown, WV 26507 USA
Dustin.Crandall@ur.netl.doe.gov

[2]Mechanical and Aeronautical Engineering Department, Clarkson University
Potsdam, NY 13699, USA
gahmadi@clarkson.edu

[3]National Energy Technology Laboratory
Morgantown, WV 26507 USA
Duane.Smith@netl.doe.gov

[4]National Energy Technology Laboratory
Morgantown, WV 26507 USA
Grant.Bromhal@netl.doe.gov

Keywords: Geological, relative permeability, CO_2 sequestration

Abstract

Geological sequestration of carbon dioxide (CO_2) is the process of placing CO_2 into subsurface formations in such a way that it will remain permanently stored. In the United States deep brine aquifers potentially provide the largest storage capability for geologically sequestered CO_2 (NETL, 2008). Within the relatively low-permeability rocks that form brine aquifers, fractures exist that can act as natural fluid conduits. Understanding how CO_2 is transported through initially liquid saturated rock fractures is important for the prediction of storage capacity and monitoring, verification and accounting of CO_2 in potential sequestration locations.

Our computational study examined the motion of immiscible fluids as they were transported through models of a fracture in Berea sandstone. The natural fracture geometry was initially scanned using micro-computerized tomography (CT) at a fine volume-pixel (voxel) resolution by Karpyn et al. (2007). This CT scanned fracture was converted into a numerical mesh for two-phase flow calculations using the finite-volume solver FLUENT® and the volume-of-fluid method. Simulations of single and two-phase flows in the reconstructed fracture geometry were performed. Initial two-phase simulations of air injection into a water saturated fracture were performed and compared to experimental results from a bench scale model manufactured using stereolithography. In both experiments and simulations the invading air moved intermittently, rapidly invading large-aperture regions of the fracture (Crandall et al. 2009). Relative permeability curves were developed to describe the motion of the two fluids. These permeability curves can be used in reservoir-scale discrete fracture models for predictions of multi-component fluid motion within fractured geological formations. The numerical model was then upgraded to better mimic the subsurface conditions at which CO_2 will move into brine saturated fractures. The simulation results show that, with the predicted lower interfacial tension between subsurface fluids, an increased volume of the less-viscous CO_2 fills the rough fracture geometry.

Introduction

Fluid movement within fractured geological media is of importance in subsurface activities including oil recovery (Selley 1998), CO_2 sequestration (Klusman 2003), geothermal energy extraction (Hanano 2004), and nuclear waste disposal predictions (Selroos et al. 2002). Fractures exist in nearly all reservoir rock formations, ranging in size from millimeters to miles. The high permeability (k) of open fractures allows for enhanced fluid mobility and greater fluid flow rates. Thus, a thorough understanding of the behavior of fluid flow through fractured porous media will enable more accurate prediction of fluid motion on the reservoir scale.

The inclusion of fractures in reservoir scale simulators requires approximations of some sort. The continuum

approach to reservoir simulation assumes that the fractures and unfractured zones of porous media can be coupled through some relationship, such as continuity of pressure between the fracture walls and the porous media (Wu et al. 2004). Discrete fracture and channel network simulators, which explicitly model flow through fracture networks, often use a Darcy's Law relationship to model fluid flow through the fractures (Seleroos et al. 2002).

Fractures may contribute to enhanced flow over regions miles in length, especially when the flow in connected fracture networks is considered (McKoy and Sams 1997). The open apertures (b) of fractures are quite small; a fracture with a mean b of 1 mm is considered large. Fracture b are defined in this study as the perpendicular distance between rock surfaces across the open fracture. The long-narrow geometry of fractures has prompted the use of "cubic-law" relations to describe flows with discrete fracture models. The cubic law is derived from the solution of the Navier-Stokes equations for momentum in a wide, narrow aperture. Simple descriptions of how fluids move through fractures are a necessary requirement for efficient reservoir scale discrete fracture models to function.

At the core-scale (i.e. cm) fractures are highly heterogeneous. Consisting of two rough surfaces in a naturally heterogeneous material, the b between walls varies throughout the fracture. Regions of zero-aperture (touching fracture walls) are common within natural fractures (Zimmerman et al. 1992, Karpyn et al. 2007). Apertures have been shown to vary significantly within fractures (Renshaw et al. 2000, Amadei and Illangasekare 1994, Dougan et al. 2000). The relative motion of fluids through individual natural fractures has been shown to be tortuous (Tsang 1984). Tortuosity (θ) of fractures has been defined as the additional distance a fluid particle must travel to circumnavigate through the heterogeneous fracture geometry. Flow through fractures has also been shown to primarily occur within 'channels' (Pyrak-Nolte et al. 1990, Brown et al. 1998), or regions of higher than average flow. Two-phase flow in fractures is affected by the tortuous fluid path and high flow rates associated with constricted regions. By identifying the parameters which cause these irregularities in the fluid flow the present study hopes to aid in the development of relationships which can be accurately used in discrete fracture models of two-phase reservoir flows.

Experimental studies (Brown 1989, Hughes and Blunt 2001, Zimmermann et al. 1992) have shown the channeling (or tortuous nature of the flow) which occurs within single natural fractures. CT scans of fractured sandstone have shown the distribution of multiple fluids within fracture to be disconnected and dependant on the fracture geometry (Rangel-German et al. 1999, Karpyn et al. 2007). Other studies have shown the relative permeability (k_r) of fractured porous media for a variety of fluid/fluid two-phase studies (Berkowitz 2002). The k_r of flow in an idealized fracture model was shown to be highly dependent on the correlation of aperture heights within fractures (Pruess and Tsang 1990). An experimental study through a single fracture has been conducted and compared to a localized cubic law model, which was shown to over predict the flow rate experimentally observed (Konzuk and Kueper 2004).

Numerical studies have been reported, and for the most part corroborate the experimental observations. Pore-level models (Section 2.1.3) have been used to show the motion of multiple fluids within idealized fracture models (Glass et al. 1998, Glass et al. 2001, Hughes and Blunt 2001) under various conditions. A percolation model was used to show the channeling affect observed in experimental studies, within a correlated aperture model (Pyrak-Nolte et al. 1990). The dispersion of tracers was shown to be affected by localized asperities within fracture (Roux et al. 1998), which was related to the properties of a macroscopic (idealized fracture) with a localized cubic-law model. Finite difference simulations of flow through realistic fracture models have shown that alteration of the fracture surface (smoothing of asperities) results in a more homogenous fluid invasion front (Lespinasse and Sausse 2000). All of these works have shown behavior different than that observed within parallel-plates, but no unifying relationship that accurately describes the flow of fluids within fractured porous media has gained widespread acceptance.

We present full Navier-Stokes simulations of single and multi-phase flows through a reconstructed CT scanned fracture. We show agreement with previously reported θ and k values and report a novel k_r relationship for air-water flows.

Nomenclature

A	Fracture cross-sectional area (m^2)
b	Fracture aperture (m)
k	Permeability (m^2)
k_r	Relative permeability (-)
L	Fracture length (m)
L_i	Particle i path length (m)
P	Pressure (Pa)
Q	Volumetric flow rate (m^3s^{-1})
W	Fracture width (m)

Greek letters

θ	Tortuosity (-)
ρ	Fluid density (kgm^{-3})
μ	Absolute viscosity (Pas)

Numerical Model

The fracture used in this study was created within a 2.59 cm diameter and 9.2 cm long core of Berea sandstone, using a modified Brazilian technique and CT scanned at Penn State University (Karypn et al. 2007). CT scanning of this fracture was performed to determine the fracture properties and to conduct flow experiments. A 240 μm voxel (volume-pixel) data set was obtained from these scans.

The 240 μm voxel data was 'cleaned' using an in-house code, which removed voids within the rock that were unconnected to the rest of the fracture. The cleaned three-dimensional fracture geometry is shown in Figure 1. A grayscale aperture map is used to show the variation in the b throughout the domain. A profile of the fracture through the midplane is shown in Figure 1 as well, with the aperture height increased to illustrate the rough fracture walls. The as-scanned fracture volume was 1216.37 mm^3 and the cleaned fracture volume was 1214.45 mm^3; a reduction of less than one percent between the two models.

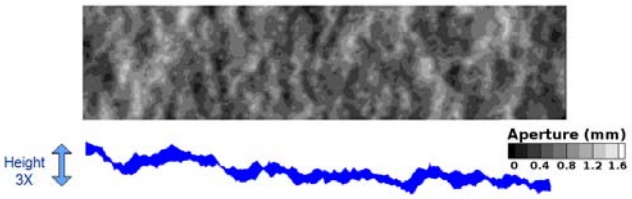

Figure1: Fracture aperture (*b*) map and rough-walled fracture profile.

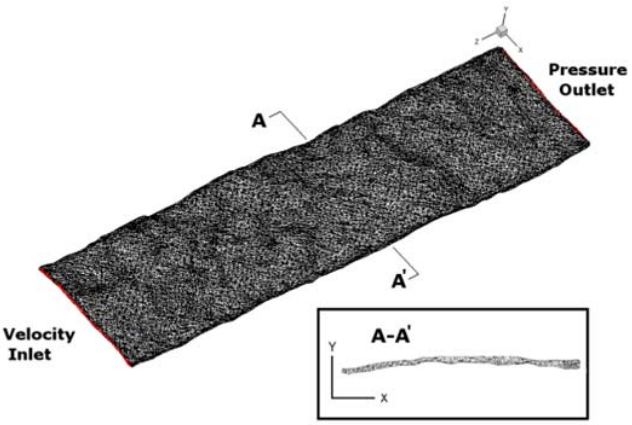

Figure 2: Computational fracture mesh.

A mesh of 688,000 unstructured tetrahedral cells was applied to the full fracture model with the pre-processor GAMBIT™. This level of mesh refinement was found to be adequate for single phase flows; two phase flow models were refined to approximately 1 million cells. The unstructured single phase model surface mesh applied to the entire fracture is shown in Figure 2, with a magnified insert of a cross-sectional profile to better illustrate the level of refinement. The inlet and outlet boundary conditions are shown as well. The surrounding fracture surfaces were treated as non-slip walls.

A series of numerical simulations were performed using the computational fluid dynamics solver, FLUENT™. Momentum was solved using a 2nd order upwind scheme, pressure was solved using the pressure staggering option scheme, pressure-velocity coupling was performed using the embedded PISO algorithm, and the volume fraction within each cell was determined with the geometric reconstruction method. The solution gradients used by these solvers were obtained by averaging node values along each cell face to obtain solutions at the cell centers. The geometries used for these analyses were three-dimensional models obtained from CT scans of a fracture in Berea sandstone by Karpyn et al. (2007). Single-phase studies to determine the fracture's θ, effective aperture b_{eff}, and effective permeability k_{eff} were conducted. Two-phase studies of the fracture were performed to determine the k_r of air and water in the fracture.

Single-Phase Flow Results

From the single phase simulations performed the θ, b_{eff} and k_{eff} have been calculated. These values have been observed to be similar to those expected for flow through a single fracture. The methods used to calculate these properties and the recorded values are discussed here.

As was previously mentioned, θ is a quantity that describes the extra distance that a fluid particle will travel as it traverses the macroscopic length of a fracture. This Lagrangian path is longer than the fracture length due to restrictions within the fracture. Thus, θ is a measurement of the heterogeneity of a fracture. To measure this with the numerical model a low injection velocity (0.1 $^{cm}/_{s}$) was applied to a single-phase flow of air through the fracture and the steady state solution was obtained. Sub-micron particles were released from the constant velocity inlet and the particles were tracked using the step-by-step particle tracker in FLUENT™ (2005). Brownian motion and gravitational forces were not included, so that the particles only followed the fluid flow. These step-by-step particle paths were exported as a tab-delineated text file and read into a spreadsheet, with the location of the particle (in Cartesian x, y, and z coordinates) written at time-steps of 10^{-8}. The distance each particle traveled between each time step, L_i, was calculated from,

$$L_i = \sqrt{(x_i - x_{i-1})^2 + (y_i - y_{i-1})^2 + (z_i - z_{i-1})^2} \qquad (1)$$

where the subscripts refer to the time steps, *i* being the current time and *i-1* the previous time. L_i was summed over the entire distance the particles traveled and these particle lengths were averaged for all the particles released; ~200 particles were evaluated over the injection face. The θ was calculated with,

$$\theta = \frac{\sum L_i}{L} - 1 \qquad (2)$$

where the fracture length L = 9.192 cm. The particles were found to travel a distance 44% greater than the fracture length, or 13.24 cm. Several representative particle paths are shown in Figure 3. Note that all the particles traveled through a narrow region near the bottom of this image, regardless of their release location. This θ value was confirmed as being a reasonable value through discussions with petroleum engineers familiar with this type of analysis (Kadambi 2006).

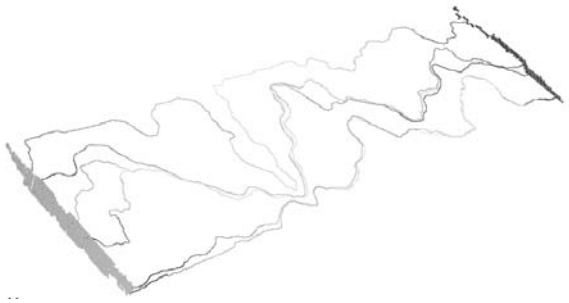

Figure 3: Representative particle pathways through fracture.

Darcy's Law for flow through porous media is often used as an approximation of flow through fracture in reservoir scale simulators (Wu et al. 2004). Darcy's Law predicts the volumetric flow rate, Q, of a fluid with viscosity μ through a porous medium with cross-sectional area A and length L

when a pressure gradient, ΔP is imposed. The k can be calculated by rearranging Equation 3.

$$Q = k\frac{\Delta PA}{\mu L} \tag{3}$$

This was accomplished with the numerical model by changing the constant rate velocity inlet shown in Figure 2 to a constant pressure inlet, imposing pressure gradients of 0.1, 1, 10, and 100 Pa across the fracture, and measuring the resultant mass flow rate of air and water through the fracture. The properties of the working fluids for these calculations are shown in Table 1. The mass flow rate was used from the FLUENT™ simulations and converted to volumetric flow rate with the densities (ρ) in Table 1. A plot of the recorded flow rates for the case of water as the working fluid are shown in Figure 4. From these results and Equation 3, the effective permeability k_{eff} of the fracture was calculated. k_{eff} refers to the fact that the fracture is not a porous medium, but the narrow b resists flow in such a manner that this relationship can be used with some accuracy. The similarities of k and k_{eff} are shown visually in Figure 5. The k_{eff} was calculated as $3.41(10^{-10})$ m^2 = 345 Darcies. This is order of magnitudes greater than the k of the surrounding sandstone (Karypn et al. 2007) and matches well to similar experimental and numerically measured fracture permeabilities.

Table 1. Fluid properties for simulations.

	ρ ($^{kg}/_{m^3}$)	μ ($^{kg}/_{m\cdot s}$)
Air	1.225	$1.8(10^{-5})$
Water	998.2	$1.003(10^{-3})$
CO2	534	$4(10^{-5})$
Brine	1052	10^{-3}

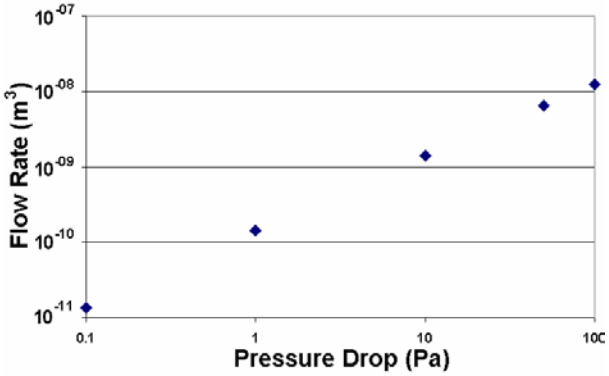

Figure 4: Volumetric flow rates of water through full fracture model.

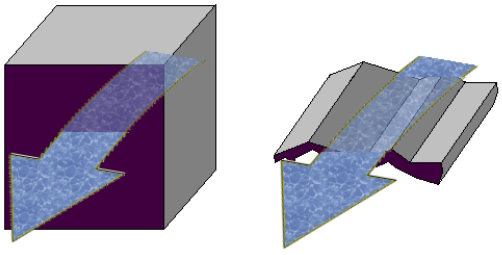

Figure 5: Permeability (k) through porous medium (left) and effective permeability (k_{eff}) through a fracture (right).

Using the same ΔP and Q results the b_{eff} of the fracture was calculated. The b_{eff} assumes that the flow through the fracture can be described by the cubic-law for flow through parallel plates. The cubic law is derived from the Navier-Stokes equations with the assumptions of a narrow b perpendicular to the flow through a wide and long set of parallel plates. This relation has been used in discrete fracture models and is given as

$$Q = -\frac{b_{eff}^3 W}{12\mu}\frac{\Delta P}{L} \tag{4}$$

The b_{eff} of the fracture was calculated as 300.4 μm from Equation (4). The similarity of this value to the smallest aperture in the fracture model (240 μm) indicates that the flow resistance within the fracture is dominated by the smallest apertures, a fact that has been previously reported in two-dimensional fracture studies (Crandall et al. 2009) and experimental studies of flow through fractures (Konzuk and Kueper, 2004).

A representative image of pressure contours through the fracture, with water as the working fluid and with an imposed pressure gradient of 15 Pa is shown in Figure 6. As can be seen the pressure drop across the fracture is non-uniform, with constricted regions reducing the pressure more rapidly. This is most apparent in the 12 Pa range of the fracture flow shown in Figure 6.

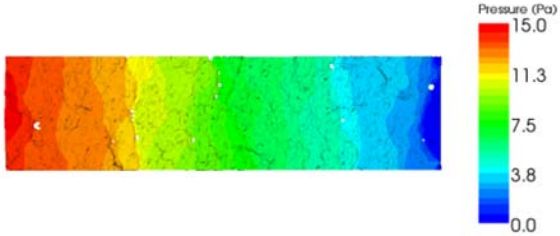

Figure 6: Pressure contours of water through fracture.

Two-Phase Flow Results

Using a refined fracture mesh simulations were performed using the Volume-of-Fluid (VOF) model. Preliminary simulations were performed using air and water as the immiscible fluids, fluid-fluid properties are listed in Table 2. To approximate fluid behavior during sequestration brine and CO_2 properties were modeled as well, with the values reported by Pashin and McIntyre (2003) for the Black Warrior Basin used to approximate the down-hole conditions. Specifically these values represent the approximate values of CO_2 and brine with a salinity of 0.085 (85000 ppm NaCl) at a pressure of 11.7 MPa and temperature of 69.6 °C. Under these conditions a γ of 35 $^{mN}/_{m}$ was modeled, based upon the reported CO_2-brine γ at reservoir conditions by Chalbaud et al. (2008).

Table 2. Fluid-fluid properties for two-phase simulations.

	Fluids	V_{in} ($^{cm}/_{s}$)	P_{out} (kPa)	γ ($^{mN}/_{m}$)	θ (°)
(a)	CO_2 - Brine	0.1	11700	35	90.0
(b)	Air – H_2O	0.1	1.01	72	80.0
(c)	Air – H_2O	1.0	1.01	72	90.0

Three images of fluid invasion into the fracture, initially filled with either water or brine are shown in Figure 7. As can be seen the saturation varies significantly with the change in the fluid-fluid properties. The brine-CO_2 system has a much lower γ, thus the capillary resistances are much lower and the invading CO_2 easily moves into small regions of the fracture. The saturations of air shown in Figure 7(b) and 7(c) show that there is a dependency of the air saturation on the direction of flow.

The relative permeabilities k_r of the fluids moving through this fracture were calculated as the permeability of each individual fluid within four equal sized segments normalized by the absolute permeability in that segment, e.g. $k_r = k_i/k$. The individual fluid permeabilities were calculated with,

$$k_i = Q_i \frac{\mu_i}{\nabla P_i} \tag{5}$$

where the subscripts indicate individual fluid properties. The pressure gradient and flow of each fluid was measured across the four individual segments of the fracture. Only when the fluid was present at both edges of a segment could the k_i be determined. This segmentation of the fracture increased the number of k_r values that could be calculated, plotted as a function of the water saturation (within each segment) in Figure 8. Several important properties of these curves are listed here. The irreducible water saturation in the first three segments was approximately 5%, 8% and 11.5%, and thus a wide range of air k_i values were recorded at these values. The k_r of air reduced sharply from ≈ 1 to nearly 10^{-5} as the water saturation increased from 0% to 30%. At water saturations of greater than 30% the invading air did not form a continuous path between segment faces and no k_i values were recorded. Conversely, the water k_r was observed to reduce dramatically at very low water saturation values, but remained fairly constant from saturations of approximately 15% to 95%. A sharp increase in the water k_r was observed as the water saturation in the segments approached 100%.

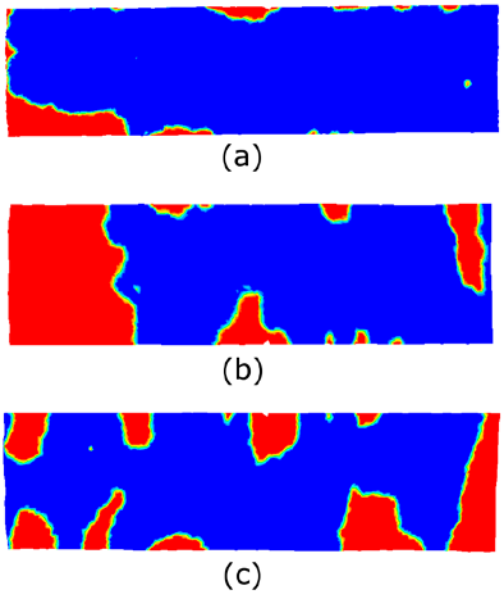

Figure 7: Two-phase flow saturations of (a) CO_2 (blue) and brine (b) air (blue) and water injected in Side 1 and (c) air (blue) and water injected in Side 2

The wide range of values obtained from this unsteady simulation of air into the water-filled fracture is shown by the all the 'calculated' points in Figure 8. Due to the sporadic motion of the invading air, Q varied dramatically for nearly identical saturation values. In a similar fashion, the pressure within the invading air changed substantially as regions of the fracture were invaded. These k_r values may be best described in terms of the probability of values at a distinct saturation, or as the range of expected values. Work is on-going to explore these ideas, as well as to identify the fluid properties that most significantly change the observed flow saturations. The averaged values shown in Figure 8 were averaged over ranges of 2% and 5% for the air and water, respectively.

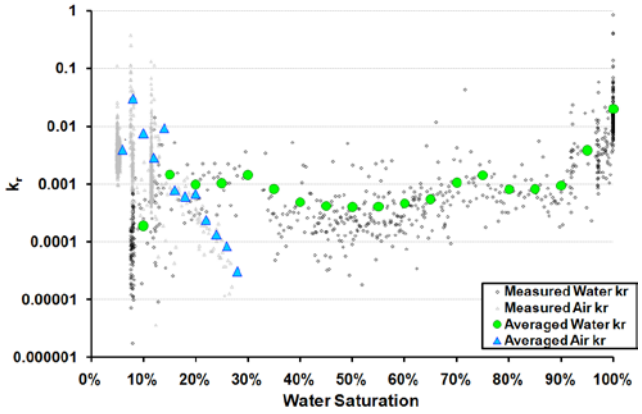

Figure 8: Relative permeability (k_r) curves of air and water within the fracture.

Conclusions

We have performed simulations of single phase and multiple phase flows in a reconstructed CT-scanned fracture. From the single phase simulations the tortuosity, effective permeability and effective aperture were all determined. Multi-phase simulations of CO_2 invading an initially brine filled fracture revealed that, with low interfacial tension values, the CO_2 tends to fill the majority of the fracture, including the small aperture locations. Similar simulations of air invading a water filled fracture, with a higher interfacial tension value, showed more fingering and less air saturation. Relative permeability curves of air invading the water filled fracture revealed a set of curves dramatically different from the typical curves for flow in porous media, due primarily to fluid-fluid interactions along the length of the fracture.

References

Amadei, B. and T. Illangasekare. 1994 A mathematical model for flow and solute transport in non-homogeneous rock fractures. Int. J. Rock Mech. Min Geomech. Abstr. 36:719-731.

Berkowitz, B. 2002. Characterizing flow and transport in fractured geological media: A review. Adv. Water Res, 25:861-884.

Brown, S.R., A. Caprihan, and R. Hardy. 1998. Experimental observation of fluid flow channels in a single fracture. J. Geophys. Res., 103:5125-5132.

Brown, S.R. 1989. Transport of fluid and electric current through a single fracture. J. Geophys. Res., 94:9429-9438.

Chalbaud, C., M. Robin, J.-M. Lombard, F. Martin, P. Egermann, and H. Bertin, 2008. Interfacial tension measurements and wettability evaluation for geological CO_2 storage, Adv. Water Resour., 32(1):98-109.

Crandall, D., G. Ahmadi, and D.H. Smith. 2010. Computational modeling of fluid flow through a fracture in permeable Rock. Transport Porous Media, In Press.

Crandall, D., G. Ahmadi, and D.H. Smith. 2009. Modeling of immiscible, two-phase flows in a natural rock fracture. Proceedings of the ASME 2009 Fluids Engineering Division Summer Meeting, FEDSM-78138.

Crandall, D., G. Ahmadi, D. Leonard, M. Ferer, and D.H. Smith. 2008. A new sterolithography experimental porous flow device. Rev. Sci. Instrum. 79(4):044501.

Dougan, L.T., P.S. Addison, and W.M.C. McKenzie. 2000. Fractal analysis of fracture: A comparison of dimension estimates. Mech. Reas. Comm., 27:383-392.

FLUENT. 2005. FLUENT 6.2 User's Guide, FLUENT Inc. Lebanon, NH.

Glass, R.J., H. Rajaram, M.J. Nicholl, and R.L. Detwiler. 2001. The interaction of two fluid phases in fractured media. Cur. Opin. Col. Int. Sci., 6:223-235.

Glass, R.J., M.J. Nicholl, and L. Yarrington. 1998. A modified invasion percolation model for low-capillary number immiscible displacements in horizontal rough walled fractures: Influence of local inplane curvature. Water Resource. Res., 34:3215-3234.

Hanano, M. 2004. Contribution of fractures to formation and production of geothermal resources. Renew. Sustain. Energy Rev., 8:223-236.

Hughes, R.G. and M.J. Blunt. 2001. Network modeling of multiphase flow in fractures. Adv. Water Res., 24:409-421.

Kadambi, J.R. 2006 Personal communication.

Karpyn, Z.T., A.S. Grader, and P.M. Halleck. 2007. Visualization of fluid occupancy in a rough fracture using micro-tomography, J. Colloid Interface Sci., 307(1):181-187.

Konzuk, J.S. and B.H. Kueper. 2004. Evaluation of cubic law based models describing single-phase flow through a rough-walled fracture. Water Res. Reas., 40:W02402.

Klusman, R.W. 2003. Rate measurements and detection of as microseepage to the atmosphere from an enhanced oil recovery/sequestration project, Rangely, Colorado, USA. App. Geochem., 18:1825-1838.

Lespinasse, M. and J. Sausse. 2000. Quantification of fluid flow: hydro-mechanical behavior of different natural rough fractures. J. Geochem. Explor., 69:483-486.

National Energy Technology Laboratory, United States Department of Energy. 2008. Carbon Sequestration Atlas of the United States and Canada, www.netl.doe.gov, 2008.

Selley, R.C. 1998. Elements of Petroleum Geology, 2nd Ed. Academic Press. Toronto, Canada.

McKoy, M.L. and Sams, W.N. 1997. Tight gas simulation: Modeling discrete irregular strata-bound fracture network flow including dynamic recharge from the matrix. Number P17, Presented at US Dept. of Energy's Natural Gas Conference, Houston TX.

Pashin, J.C. and M.R. McIntyre. 2003. Temperature-pressure conditions of the Black Warrior basin: implications for carbon sequestration and enhanced coalbed methane recovery, Int. J. Coal Geol. **54**(3):167-183.

Pruess, K. and Y.W. Tsang. 1990. On two-phase relative permeability and capillary pressure of rough-walled fractures. Water Res. Reas., 26:1915-1926.

Pyrak-Nolte, L.J., D.D Nolte, L.R. Myer, and N.G.W. Cook. 1990. Fluid flow through single fractures. In *Rock Joints*, ed. Barton and Stephansson, Balkema, Rotterdam, 405-412.

Rangel-German, E., S. Akin, and L. Castanier. 1999. Multiphase-flow properties of fractured porous media. *SPE 54591*, Presented at 1999 SPE Western Regional Meeting, Anchorage, Alaska, May 26-28.

Renshaw, C.E., J.S. Dadakis, and S.R. Brown. 2000. Measuring fracture apertures: A comparison of methods. Geophys. Res. Lett., 27:289-292.

Roux, S., F. Plouraboué, and J.-P. Hulin. 1998. Tracer dispersion in rough open cracks. Trans. Porous Media, 32:97-116.

Tsang, Y.W. 1984. The effect of tortuosity on fluid flow through a single fracture. Water Resour. Res., 4W0827:1209-1215.

Wu, Y.-S., L. Pan, and K. Preuss. 2004 A physically based approach for modeling multiphase fracture-matrix interaction in fractured porous media. Adv. Water Res., 27:875-887.

Zimmerman, R.W., D.W. Chen, and N.G.W. Cook. 1992. The effect of contact area on the permeability of fractures. J. Hydrology, 139:79-96.